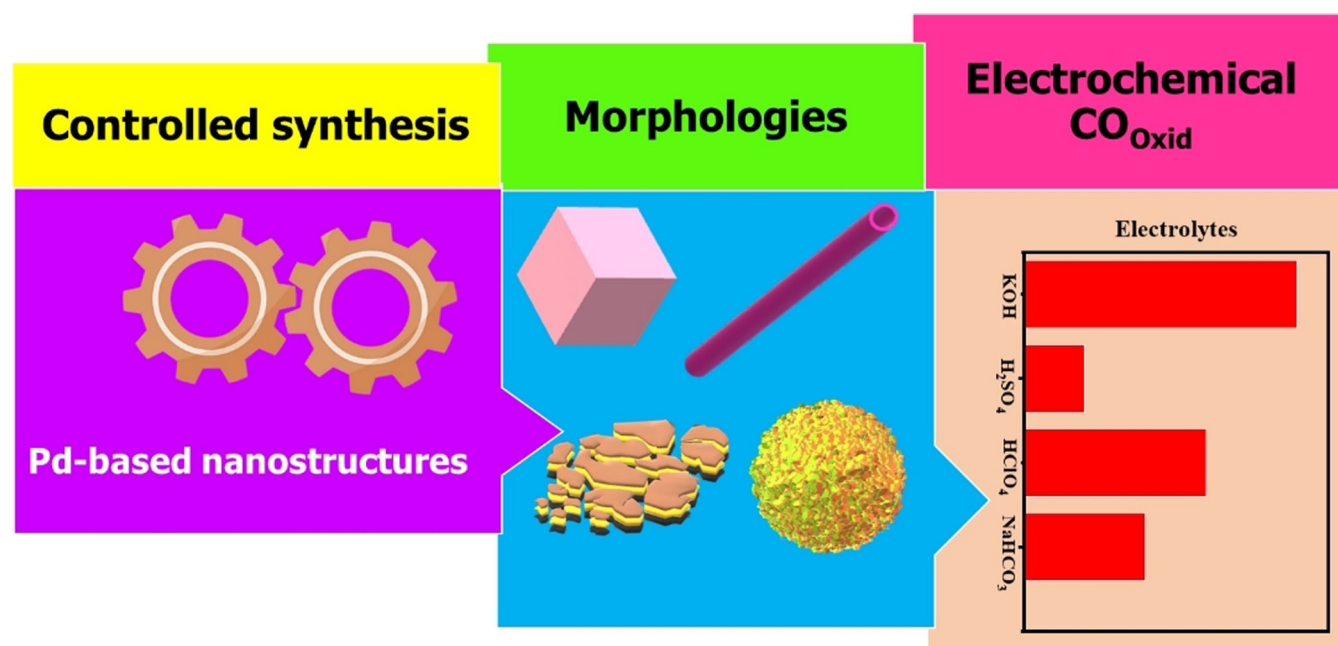


Special
Collection

Controlling the Synthesis Protocols of Palladium-Based Nanostructures for Enhanced Electrochemical Oxidation of Carbon Monoxide: A Mini-Review

Adewale K. Ipadeola,^[a, b] Kamel Eid,^{*[b]} Aderemi B. Haruna,^[c] Aboubakr M. Abdullah,^{*[a]} and Kenneth I. Ozoemena^{*[c]}



Pd-based nanostructures are endowed with impressive catalytic features for alcohol-based fuel cells, however, their poisoning by carbon monoxide (CO) is a great barrier to large-scale utilization of such fuel cells as alternative power sources. The need to optimize the electrochemical CO oxidation (CO_{Oxid}) of Pd-based nanostructures in various electrolytes has attracted much attention in the last decade, so it is important to provide a timely update on this area of research. This mini-review

highlights the most recent advances in controlling some synthesis methods of Pd-based nanostructures and their morphologies for enhanced electrocatalytic CO_{Oxid} in different electrolyte conditions in the last three years. Finally, the main challenges for commercially viable Pd-based nanostructures for electrochemical CO_{Oxid} are discussed, highlighting the future perspectives and providing promising solutions for practical CO_{Oxid} application.

1. Introduction

Catalytic carbon monoxide oxidation (CO_{Oxid}) is of great importance in various industrial and environmental applications because it is an extraordinary probe for assessing catalysts' activity in heterogeneous catalysis and conversion of hazardous gas to less toxic products. Also, CO_{Oxid} is important in fuel cells and energy conversion (i.e., alcohol fuel cells), because it is a common impurity that poisons the catalysts, leading to reduced performance, so electrochemical CO_{Oxid} can be employed as a pre-treatment step to remove CO from the fuel stream before it enters the fuel cell to enhance the overall efficiency and longevity of fuel cells. The CO_{Oxid} is usually achieved by thermal, electrochemical, and photoelectrochemical methods in the presence of various catalysts (i.e., noble metals, transition metals, and quantum dots).^[1–3] Although the thermal process is the most common in the industry, its high energy demand (i.e. heating to elevated temperature) is a great barrier,^[4,5] whilst the electrochemical CO_{Oxid} is less energy demand (i.e., it occurs at room temperature and atmospheric pressure) and meets the sustainability requirements.^[6–8] Unlike other electrocatalysts (i.e., PtRu, PtSn, Pt/metal oxide, and Rh N₄), Pd-based catalysts have better tolerance to CO poisoning, particularly in alkaline conditions.^[9,10] Also, Pd-based catalysts are among the commercially available catalysts for various

electrocatalytic oxidation/reduction reactions, so it is important to highlight the electrochemical CO_{Oxid} activity of Pd-based catalysts. Pd-based catalysts are imminent with their impressive catalytic activity towards electrochemical CO_{Oxid} , due to their unique ability to induce the activation/dissociation of reactants and ease the formation of reactive oxygenated species (i.e., *OH) from the electrolytes at low potential, resulting in quick CO_{Oxid} kinetics.^[6–8]

Also, Pd-based catalysts are endowed with impressive properties (i.e., great electrochemical active surface area, low density, quick charge mobility, and ease adsorption/diffusion of reactants) that benefit CO_{Oxid} electrocatalysis.^[11,12] To defeat the high-cost and earth-rarity of Pd metal, it is usually mixed with other low-cost and earth-abundant metals/metal oxides (i.e., Co, TiO₂, SiO₂, Ce₂O₃, Fe₂O₃, Ni, Fe, Cu).^[13–17] This not only reduces the usage of Pd but also modulates the d-band center of Pd (i.e., upshifting or downshifting), resulting in accelerating the CO_{Oxid} kinetics at low potential and facilitating desorption of intermediates/products.

The research related to Pd-based catalysts for CO_{Oxid} led to 4651 articles in the last decade, including 59 publications for electrochemical CO_{Oxid} , which were cited 2751 times (~46.63 citations per article) according to the Web-of-Science survey (Figure 1a). However, no review emphasized the electrocatalytic CO_{Oxid} on Pd-based nanostructures as far as we found. Thus, it is pertinent to provide timely updates on this area of research with focus on the effect of fabrication strategies (i.e., microwave-irradiation, hydrothermal/solvothermal, chemical reduction), morphologies (i.e., nanosheets, nanorods, nanoclusters), and electrolytes (HClO₄, H₂SO₄, KOH, NaHCO₃) on the electrocatalytic CO_{Oxid} performance of Pd-based catalysts (Figure 1b).

2. Fundamentals of Electrocatalytic CO Oxidation


The electrochemical CO_{Oxid} activity is usually probed using various electrochemical techniques, including cyclic voltammetry (CV), linear sweep voltammetry (LSV), chronoamperometry (CA) and electrochemical impedance spectroscopy (EIS) using three-electrode systems in different electrolytes saturated with CO gas at room temperature and atmospheric pressure. These techniques determine the performance indicators (i.e., onset/oxidation potentials ($E_{\text{Onset}}/E_{\text{Oxid}}$), overpotential potential (η), peak oxidation current density (j_{Oxid}), electro-

[a] Dr. A. K. Ipadeola, Prof. A. M. Abdullah
Center for Advanced Materials
Qatar University
Doha 2713 (Qatar)
E-mail: bakr@qu.edu.qa

[b] Dr. A. K. Ipadeola, Dr. K. Eid
Gas Processing Center(GPC)
College of Engineering
Qatar University
Doha 2713 (Qatar)
E-mail: kamel.eid@qu.edu.qa

[c] Dr. A. B. Haruna, Prof. K. I. Ozoemena
Molecular Sciences Institute
School of Chemistry
University of the Witwatersrand
Private Bag 3, PO Wits, Johannesburg 2050 (South Africa)
E-mail: kenneth.ozoemena@wits.ac.za
Homepage: <http://www.wits.ac.za/staff/academic-a-z-listing/o/kennethozoemena@wits.ac.za/>

 This article is part of a Special Collection on Electrochemistry in Africa

 © 2023 The Authors. ChemElectroChem published by Wiley-VCH GmbH. This is an open access article under the terms of the Creative Commons Attribution License, which permits use, distribution and reproduction in any medium, provided the original work is properly cited.

chemical active surface area (ECSA), mass activity (MA), specific activity (SA), CO_{Oxid} reaction rate (i.e., apparent heterogeneous electron transfer rate constant) and durability.

The onset potential (E_{Onset}) is the potential just above the current density (0 mA/cm²), while oxidation potential (E_{Oxid}) is the potential at the CO_{Oxid} peak. Both E_{Onset} and E_{Oxid} can easily be determined from the LSV curves and could be presented in terms of overpotential (η), defined in equation 1 (Equation 1). The lower the values of E_{Onset} , E_{Oxid} and η , the better the activity of catalyst.

$$\eta = (\text{applied potential} - \text{standard reduction potential of the reference electrode}) \quad (1)$$

The MA is calculated by normalizing the CO_{Oxid} current (i_{Oxid}) to the loading of Pd on the working electrodes (m_{Pd}) using Equation 2.

$$\text{MA} = \frac{i_{\text{Oxid}}}{m_{\text{Pd}}} \quad (2)$$

The SA is calculated by normalizing the MA to the ECSA using Equation 3.

$$\text{SA} = \frac{\text{MA}}{\text{ECSA}} \quad (3)$$

The ECSA via normalizing the charge from the integration of CO adsorbed in the forward direction (Q_{CO}) to the m_{Pd} and



Dr. Adewale Kabir Ipadeola obtained his B.Sc. (2012) M.Sc. (2015) and Ph.D. (2020) in Chemistry from the Lagos State University, University of Lagos, and University of the Witwatersrand, respectively. He is presently a Postdoctoral Researcher at the Center for Advanced Materials, Qatar University with research interests in electrocatalysis, green energy production, and greenhouse gas conversion to value-added products. Dr. Ipadeola has over nine years of experience in teaching and research and has published over 35 peer-reviewed articles.



Kamel obtained his bachelor's degree from Al-Azhar University (Egypt, 2005), his master's degree from Helwan University (Egypt, 2011), and his Ph.D. degree from the Chinese Academy of Sciences (China, 2016). He worked at several universities, like the American University, Changchun Institute of Applied Chemistry (China), and Zhejiang University of Technology (China) before moving to Qatar University in 2019. He has published over 100 research papers, one book with the RSC (London), filled 15 USA-granted patents, and participated in 31 international conferences (h-index 34). His current work includes developing nanosystems for green energy production and greenhouse gas conversion into useful materials.



Aderemi Haruna is currently a Research Associate with the Ozoemena group at the University of the Witwatersrand (Wits), Johannesburg, South Africa. His research interests lie in the fields of energy storage, electrochemistry and materials science, with a focus on lithium-ion, lithium-sulphur, sodium-ion and zinc-air batteries. He is also interested in exploring green chemistry synthetic methods (especially microwave irradiation) aimed at tuning the physico-chemistry and electrochemical properties for material production. He holds a PhD (chemistry) from Wits, specialising in materials electrochemistry and manganese-based cathode materials for lithium-ion batteries.



Prof. Aboubakr Abdullah has 30 years of experience in academia and industry. He published more than 200 peer-reviewed articles and conference proceedings in addition to many USA-granted patents. He earned his Ph.D. (2003) from the Pennsylvania State University. Since he joined Qatar University (2012), he has managed more than ten research mega-projects funded by different agencies, e.g., Qatar National Research Fund (QNRF), Qatar University, Hydro/Qatalum, Qatar Power (QP) and Qatar Shell (QS). Also, he offered many consultations for different companies, e.g., Qatar Gas, Qatalum, Qatar Electricity and Water Company (QEWC), and Kahramaa. In 2020, he won the Qatar University's Research Excellence Award – "Science and Engineering Path".



Prof. Kenneth I. Ozoemena is a Research Professor at the University of the Witwatersrand (Wits) where he leads the prestigious South African SARChI Chair in Materials Electrochemistry and Materials Technologies (MEET), supported by the Department of Science and Innovation (DSI) and the National Research Foundation (NRF). His current research activities are in energy storage and conversion systems, and electrochemical sensors. He holds a PhD (Chemistry) from Rhodes University (2003). He has more than 15 years' research experience as an electrochemist, including working at the Council for Scientific and Industrial Research (CSIR) as a Chief Research Scientist for 8 years. He spent a year at Cornell University, USA, as a Senior Visiting Scholar, working with the Abruña group (2022-2023). He has received several awards, including the NRF's A-rating as an international scholar. He is a member of the Academy of Science of South Africa (ASSAf), Fellow of the African Academy of Science (FAAS), and Fellow of the Royal Society of Chemistry (FRSC). He is the co-Editor-in-Chief of the Electrochemistry Communications.

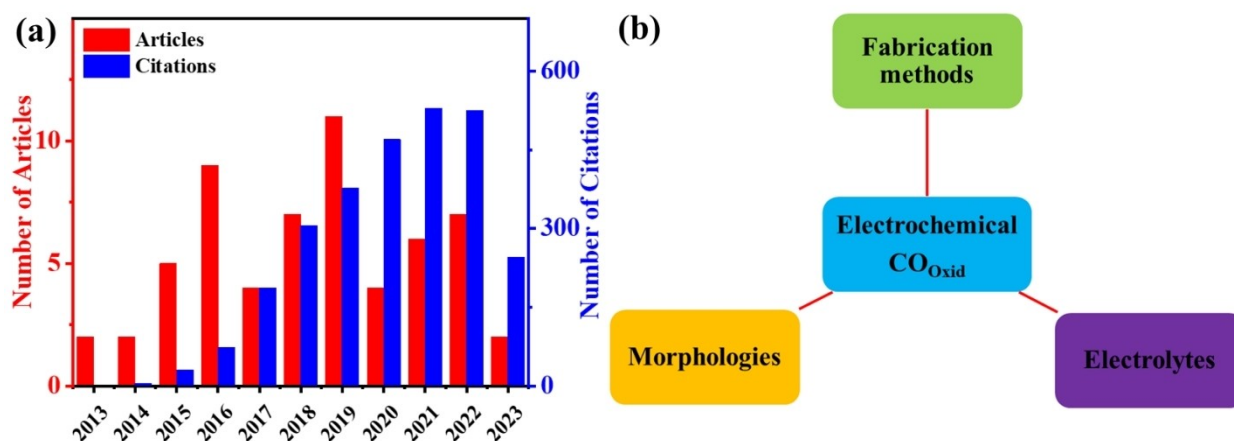


Figure 1. (a) Number of published articles/citations in the last 10 years from the Web-of-Science with keywords “Pd catalysts electrochemical CO_{oxid}” and (b) review focus.

charge assigned to the CO coverage on monolayer Pd's surface (420 μC/cm²) using Equation 4

$$ECSA = \frac{Q_{CO}}{m_{Pd} \times 420} \quad (4)$$

Measuring the CO_{oxid} current density (j_{Oxid}) at different scan rates and plotting the j_{Oxid} vs. square root of scan rate ($v^{1/2}$), following the Randles-Sevcik equation enable the determination of diffusion-coefficient of electroactive species and stoichiometry of redox processes is estimated from the slope.

The fitting of EIS Nyquist plots is important to determine the solution resistance, charge transfer resistance (R_{ct}), constant phase element, and Warburg (W_d) which are the main indicators for the charge mobility, ionic conductivity, electrolyte-electrode interaction, and CO_{oxid} kinetics.

The apparent heterogeneous electron transfer rate constant (k_{app}) for CO_{oxid} is inversely related to R_{ct} via Equation 5.

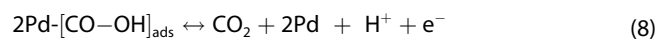
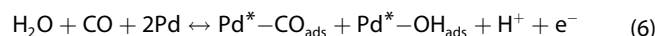
$$k_{app} = \frac{RT}{n^2 F^2 A C R_{ct}} \quad (5)$$

Where universal gas constant ($R=8.3145$ J/mol/K), absolute temperature (T), number of electron transfers ($n=1$), Faraday constant ($F=96484.33$ C), geometric area of the electrode (A (cm²)), concentration of the solution (C (mol/cm³)), and charge transfer resistance (R_{ct} (Ω)).

The durability of the catalysts for the CO_{oxid} is a crucial parameter for practical use, which can be performed with chronoamperometry at the E_{Oxi} for a long time and/or accelerated stability test with multiple cycles of CV curves. An excellent catalyst will have an insignificant deviation from the initial voltammogram after the durability without any morphological changes.

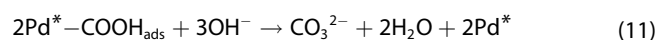
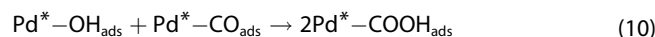
The CO_{oxid} mechanism on Pd-based catalysts in the acidic electrolyte (i.e., HClO₄ and H₂SO₄) mostly proceeds via Langmuir-Hinshelwood, which involves the co-adsorption of CO_{ads} and OH_{ads} on Pd active sites. This is followed by the

formation of CO₂ via the concurrent desorption of CO_{ads} and OH_{ads} and subsequent formation of CO₂ and regeneration of the Pd (Equations 6–8).^[18–21]



Where “*” represents the active site of the Pd-based catalyst.

The CO_{oxid} mechanism of Pd-based catalysts in the alkaline electrolyte (i.e., KOH) mostly proceeds via Equations 9–11.^[22,23]



Mechanistically, structural modification of Pd-based catalysts (i.e., 1D nanorods, 2D nanosheets, 3D hollow spheres, core-shell, etc.) enables abundant active sites, improved electronic states and optimized reactants (CO + OH) adsorption/activation and CO₂ desorption, which are advantageous for boosting CO_{oxid} electrocatalysis, via ligand, strain and ensemble effects.^[24]

3. Development of Pd-Based Nanostructures for Electrochemical CO Oxidation

3.1. Rational Design and Synthesis of Pd-Based Nanostructures

There are various approaches for tailoring the morphology and composition of Pd-based catalysts, such as chemical reduction, template-based, galvanic replacement, hydrothermal, and microwave irradiation, following various formation mechanisms, like Kirkendall, selective-etching, oriented attachment growth, and nucleation/growth.^[25,26] These methods varied in their efficiency to produce various nanostructures (i.e., cubes, wires, dendritic, and polyhedrons), but template-based, including soft-templates (i.e., triblock-copolymer surfactants and liquid-crystals), hard template (i.e., silica, polymers, anodic oxidized metal, and carbon) and hybrid are the most effective for the production of well-defined porous structures with controlled porosity (i.e. pore size and pore volume), shapes, and surface area.^[27] However, the high cost, use of hazardous chemicals, and multiple reaction steps are the main drawbacks of template-based methods. Despite the sensible advances in the formation methods of Pd-based catalysts, the high mass production (i.e., several kilograms per one run) remains a grand challenge and is not yet reported,

which subsequently cannot meet the large-scale applications. Table 1 summarizes the electrochemical CO_{Oxid} of Pd-based electrocatalysts.

3.2. Electrocatalytic CO oxidation (CO_{Oxid})

The electrocatalytic CO_{Oxid} is a crucial parameter for the optimal functioning of fuel cells, environmental sustainability and synthetic gas in industries.^[28–31] The sluggishness of CO_{Oxid} necessitates the utilization of highly active and durable electrocatalysts. Various approaches are utilized for the deliberate fabrication of Pd-based nanostructures, comprising the combination of ultra-low Pd with one or more other metals, that enable augmented physicochemical merits (i.e., porosity, surface area, electron density, d-band center, defects, electrical conductivity) and electrocatalytic features (i.e., favourable adsorption/activation of CO and H₂O splitting to generate ⁻OH at low overpotential) for excellent CO_{Oxid} electrocatalysis in different electrolytes.^[32–36]

Binary PdM-based nanostructures with metal-oxides and/or carbon-based supports are impressive electrocatalysts in fuel cells and satisfactory CO_{Oxid}. For example, zeolitic imidazole frameworks (ZIF-67) containing Co-N_x prepared by microwave-irradiation (MW-I), carbonization and etching were utilized as support for Pd nanocrystals growth (Pd/ZIF-67/C) by

Table 1. Pd-Based Nanostructures for Electrocatalytic CO Oxidation.

Catalysts	Synthesis method	Morphology	Electrolytes	E_{Oxid} [V]/ j [mA/cm ²]	Ref.
Pd/ZIF-67/C	MW-I/calcination/ etching/MW-I	Spherical Pd on porous nanosheets	0.1 M HClO ₄ 0.1 M KOH 0.1 M NaHCO ₃	0.95 _{RHE} /4.12 0.76 _{RHE} /3.78 0.85 _{RHE} /1.50	[37]
Pd/Ni-MOF/PC	MW-I/calcination/ etching/MW-I	Spherical Pd on porous nanosheets	0.1 M HClO ₄ 0.1 M KOH 0.1 M NaHCO ₃	1.05 _{RHE} /4.71 0.74 _{RHE} /3.94 0.83 _{RHE} /1.22	[38]
Pd/T ₃ C ₂ T _x	Etching/deamination/ impregnation	Semi-spherical Pd on 2D nanosheets	0.1 M HClO ₄	0.90 _{Ag/AgCl} /0.318	[41]
PtPd/CNs	Ultrasonic treatment/ annealing	1D nanorods	0.1 M KOH	-0.19 _{Ag/AgCl} /14.75	[39]
Au/Pd/gC ₃ N ₄ NTs	Protonation/ annealing	Nanotubes	0.1 M KOH	-0.60 _{Ag/AgCl} /15.50	[40]
Pd-NbN/C	Solvothermal	Spherical Pd on nanosheets	0.5 M H ₂ SO ₄	0.91 _{RHE} /-	[42]
Pd-PdW HSs/C	Hydrothermal	Spherical Pd on nanosheets	0.5 M H ₂ SO ₄	0.780 _{SCE} /-	[43]
3Pd/1Au alloy	Electrodeposition	Nanoflowers	0.1 M HClO ₄	0.92 _{RHE} /-	[44]
PdCoH NSs	Solvothermal	2D Curly Nanosheets	1.0 M NaOH	-0.20 _{Hg/HgO} /0.5	[45]
N-Pd ₆₀ Cu ₄₀ NS	N ₂ -plasma-treatment	Interconnected nanosheets	1.0 M KOH	-0.160 _{Hg/HgO} /-	[46]
PdNi	Chemical-reduction	Foam-like with connected nanosheets	1.0 M KOH	-0.200 _{Ag/AgCl} /1.88	[47]
Ir-SAs/Pd	Chemical-reduction	Cuboctahedral	1.0 M KOH	-0.150 _{SCE} /0.20 mA	[48]
PdNiO-CeO ₂ /OLC	Sol-gel/Impregnation	Spongy-like Pd on flower-like shaped CeO ₂ /OLC	0.1 M HClO ₄ 0.1 M KOH 0.1 M NaHCO ₃	1.10 _{RHE} /2.50 0.79 _{RHE} /2.49 0.88 _{RHE} /1.23	[49]
PdNiO-CeO ₂ /CB	Sol-gel/Impregnation	Spherical Pd on flake-like shaped CeO ₂ /OLC	0.1 M HClO ₄ 0.1 M KOH 0.1 M NaHCO ₃	1.05 _{RHE} /2.65 0.80 _{RHE} /2.54 0.87 _{RHE} /0.85	[50]

KEY: Reversible hydrogen electrode (RHE), Porous carbon (PC), microwave-irradiation (MW-I), onion-like-carbon (OLC), carbon-black (CB).

MW-I (Figure 2a). The Pd/ZIF-67/C with spherical Pd on porous nanosheet structures, proven by SEM (Figure 2b) delivered superior CO_{Oxid} activity in 0.1 M HClO_4 , 0.1 M KOH, and 0.1 M NaHCO_3 by 4.2-, 4.4- and 4.0-folds of Pd/C and 2.7-, 3.6- and 2.7-folds of Pt/C (Figures 2c–2e), owing to the rich active-sites, reduced d-band center and optimal utilization of Pd/Co- N_x .^[37] Similarly, Ni-MOF-derived hierarchical porous carbon nanosheets decorated with spherical Pd nanocrystals (Pd/Ni-MOF/PC) had significantly increased CO_{Oxid} in varied media (HClO_4 , KOH and NaHCO_3) relative to its analogue without etching (Pd/Ni-MOF/C) and Pd/C, besides its superior stability, attributable to its abundant active sites of Pd/Ni- N_x and porous defective MOF/PC beneficial for facile CO activation and H_2O dissociation to generate OH^- species at lower potentials.^[38] These studies revealed the potential of metal-organic framework (MOF-based supports) for Pd nanostructures for boosted CO_{Oxid} kinetics.

$\text{Ti}_3\text{C}_2\text{T}_x$ ordered/exfoliated 2D nanosheets anchored semi-spherical Pd nanoparticles (Pd/ $\text{Ti}_3\text{C}_2\text{T}_x$, 2.5 wt.%) were prepared by HF-etching and impregnation.^[41] The Pd/ $\text{Ti}_3\text{C}_2\text{T}_x$ showed a CO_{Oxid} activity in 0.1 M HClO_4 with $E_{\text{Oxid}}/j_{\text{Oxid}}$ (0.9 V/0.318 mA/cm^2), due to the coupling of physicochemical merits of $\text{Ti}_3\text{C}_2\text{T}_x$ and catalytic features of Pd, while $\text{Ti}_3\text{C}_2\text{T}_x$ was CO_{Oxid} inactive. This study revealed the impressive ability of $\text{Ti}_3\text{C}_2\text{T}_x$ Mxene to act as a reducing agent for the formation of Pd

nanoparticles without the need for a reducing agent and could open the way for the utilization of $\text{Ti}_3\text{C}_2\text{T}_x$ as a support for Pd-based electrocatalysts in CO_{Oxid} . The fabrication of atomically Pt-/Pd-co-doped carbon nitrides (PtPd/CNs, 1.5 wt.%) via protonation of melamine with NaNO_3/HCl /ethylene-glycol and annealing (550 °C, 2 h; N_2), led to the rapid formation of 1D nanorods (94 ± 2 nm) revealed by SEM (Figure 2f) and high surface area (155.2 m^2/g), which are maximally utilized for its excellent CO_{Oxid} in 0.1 M KOH with high j_{Oxid} (14.75 mA/cm^2) that was 2.01-folds of commercial-Pt/C and 23.41-folds of CNs (Figure 2g).^[39] Also, UV-visible irradiation further increased the CO_{Oxid} by ~ 1.5 -times (Figure 2h), owing to the coupling of catalytic merit of PtPd and physicochemical features of 1D CNs. This study could allow the utilization of CNs as a support for Pd-based catalysts in CO_{Oxid} . The controlled preparation of Au/Pd/ gC_3N_4 with nanotubes (NTs) was evidenced by TEM (Figure 2i), which gave outstanding CO_{Oxid} in 0.1 M KOH with (~ 15.5 mA/cm^2) in 0.1 M KOH than the gC_3N_4 and even PtPd/CNs (Figure 2j), due to the improved electronic structures of Au/Pd, high electron density, conductivity, more accessible surface area for facile CO adsorption and activation/dissociation of H_2O to generate active O-containing species.^[40] More PdM/ gC_3N_4 needs to be explored for excellent CO_{Oxid} .

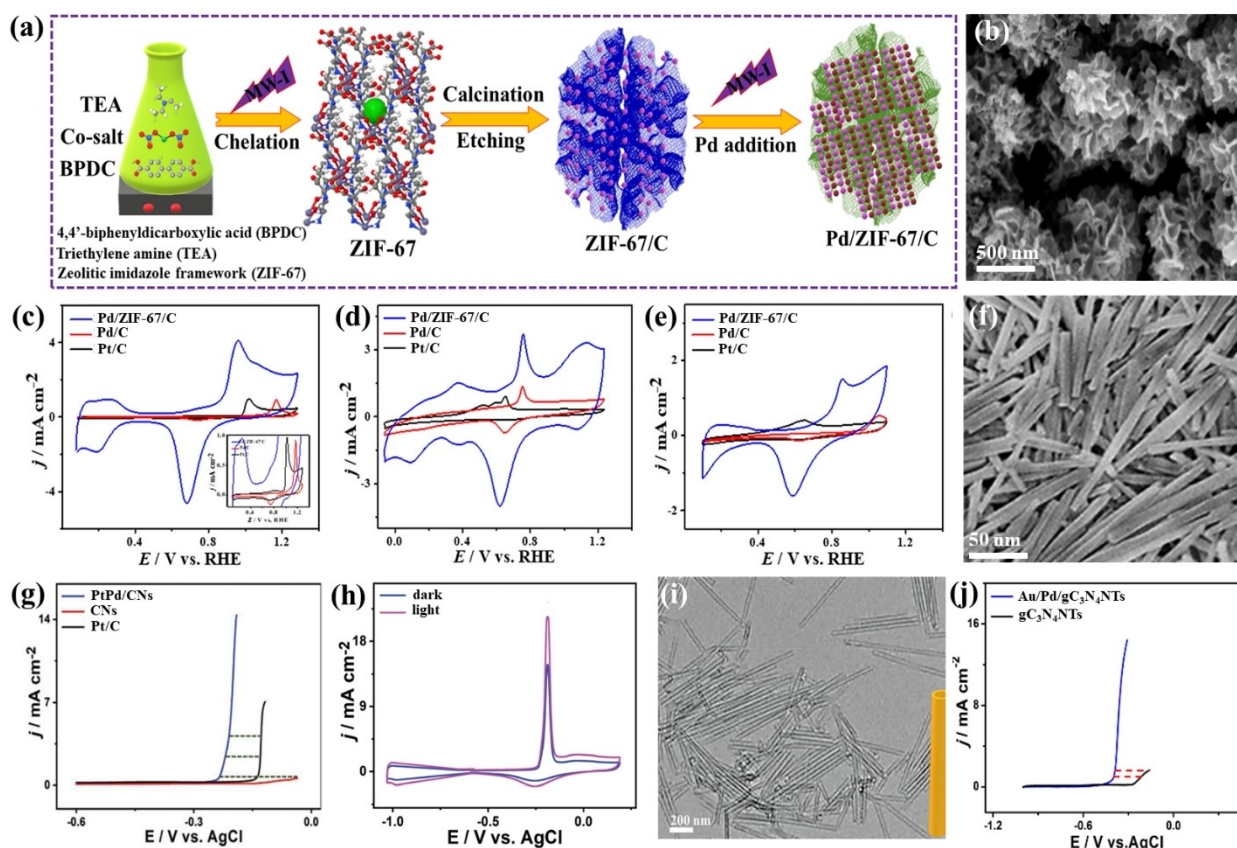


Figure 2. (a) Synthetic scheme, (b) SEM, CV curves in (c) 0.1 M HClO_4 , (d) 0.1 M KOH, and (e) 0.1 M NaHCO_3 of Pd/ZIF-67/C. “Adapted with permission from Ref.: [37] Copyright (2022) the American Chemical Society”. (f) SEM, (g) LSV and (h) CV 0.1 M KOH with/without UV-visible light of PtPd/CNs. “Reprinted with from Ref.: [39] Copyright (2019) the Royal Society of Chemistry”. (i) TEM and (j) LSV in 0.1 M KOH of Au/Pd/ gC_3N_4 NTs. “Reproduced with permission from Ref.: [40] Copyright (2019) the American Chemical Society”.

A series of nitrides-modified Pd/C (i.e., Pd-NbN/C, Pd-Mo₂N/C, Pd-VN/C, and Pd-BN/C) with spherical Pd on nanosheets were synthesized by solvothermal (120 °C; 5 h) method.^[42] This study revealed that the Pd-NbN/C had moderate CO adsorption and easily removed, resulted in CO_{Oxid} activity 0.5 M H₂SO₄ with trend of E_{Oxid} : Pd-NbN/C (0.905 V) < Pd-Mo₂N/C (0.909 V) < Pd-VN/C (0.930 V) < Pd-BN/C (0.947 V) < Pd/C (0.950 V). Hydrothermal (140 °C; 1.5 h) synthesis of W-doped Pd spheres grown and Pd nanocrystals/C nanosheets (Pd-PdW HSs/C) using DMF/acetic acid and CO as reducing and structure-directing agent.^[43] The Pd-PdW HSs/C gave the best CO_{Oxid} activity at E_{Oxid} (0.70 V_{SCE}) relative to Pd NSs/C (0.75 V_{SCE}), Pd NCs/C (0.74 V_{SCE}) and commercial-Pd/C (0.77 V_{SCE}), which was attributed to its modified electronic structure and epitaxial heterostructures.

Free-standing binary PdM-based nanostructures have excellent CO_{Oxid} in various electrolytes. For instance, Pd-Au (1:1, 3:1, 1:3) bimetallic nanocatalysts were fabricated by electrodeposition in choline/urea deep eutectic solvents (DESs), where 3Pd/1Au exhibited nanoflower-shaped alloys, reduced size, and enhanced surface area that gave higher CO_{Oxid} at E_{Oxid} (0.92 V_{RHE}) than 1Pd/1Au (1.0 V_{RHE}) and 1Pd/3Au (1.1 V_{RHE})

because increased Au suppressed reactive oxygenated species adsorption and hydrogen adsorption/desorption.^[44] The introduction of oxophilic metal and interstitial hydrogen into Pd (PdCoH NSs) was made by solvothermal (200 °C; 1 h) method with DMF as solvent/reductant, while Mo(CO)₆ directed the formation of 2D curly nanosheets, proved by HAADF-STEM (Figure 3a) that enabled its improved surface area coupled with its modulated d-band center, evidenced by XPS valence-band (Figure 3b) for excellent CO_{Oxid} in 1.0 M NaOH at lower E_{Oxid} /high j_{Oxid} (−0.20 V_{Hg/HgO}/ 0.50 mA/cm²) relative to PdCo NSs (−0.17 V_{Hg/HgO}), PdH NSs (−0.15 V_{Hg/HgO}) and commercial-Pd/C (−0.15 V_{Hg/HgO}) (Figure 3c).^[45]

The construction of surface nitride PdCu (N-Pd₆₀Cu₄₀ NSs) via nitrogen-plasma treatment (Figure 3d) enabled interconnected nanosheet morphology proved by SEM (Figure 3e), improved electronic/structural effects and charge transfer that weakened the adsorption of CO-like intermediates, leading to higher CO_{Oxid} at E_{Oxid} (−0.16 V_{Hg/HgO}) than Pd₆₀Cu₄₀ NSs (−0.15 V_{Hg/HgO}), N-Pd NSs (−0.13 V_{Hg/HgO}), Pd NSs (−0.12 V_{Hg/HgO}) and commercial-Pd/C (−0.10 V_{Hg/HgO}) (Figure 3f).^[46] Self-standing PdM (M = Ni, Fe and Co) were synthesized by aqueous-solution reduction with NaBH₄ in an ice bath.^[47] Amongst the porous

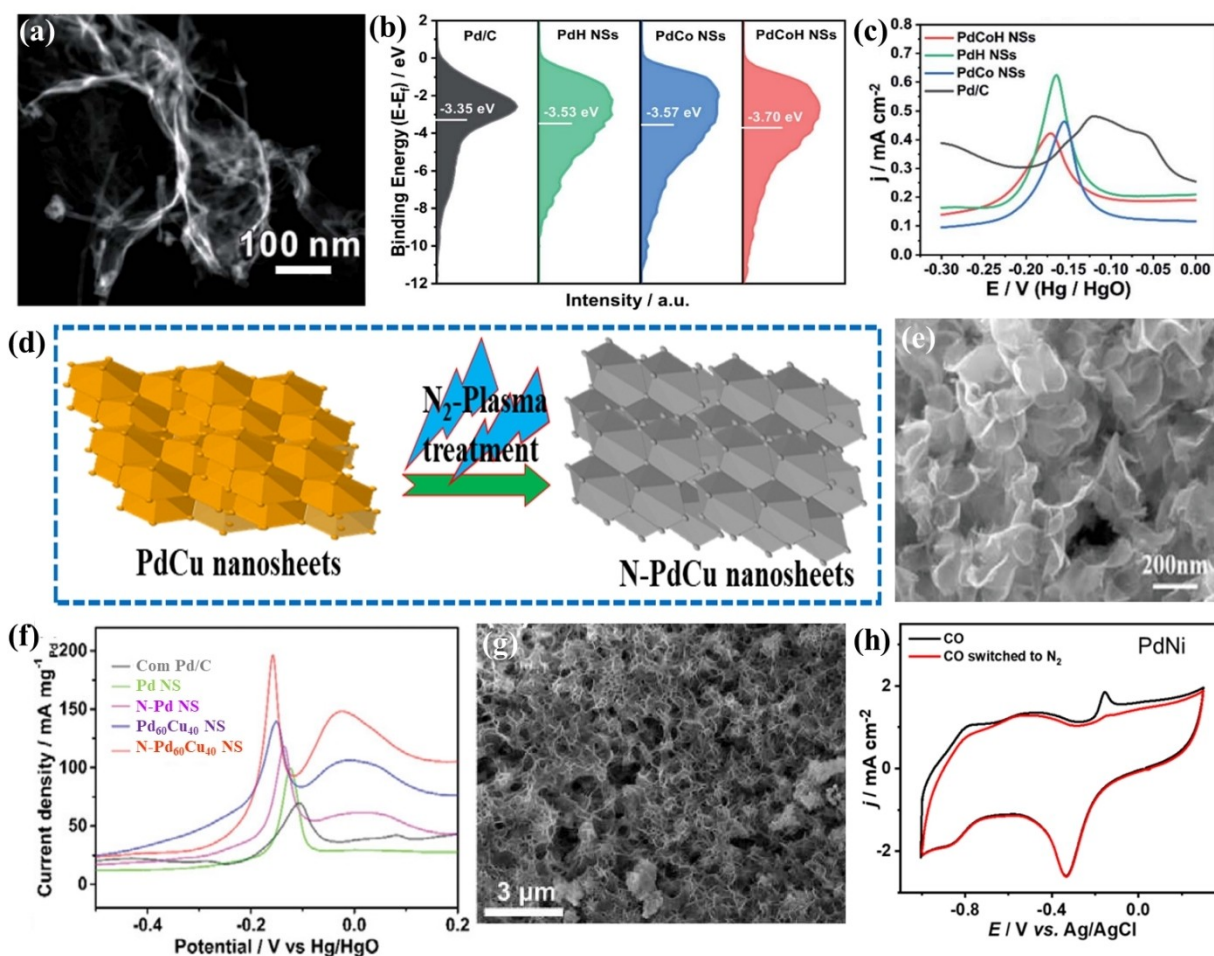


Figure 3. (a) HAADF-STEM, (b) XPS valence-band and (c) CV of PdCoH NSs. Reprinted with permission from Ref.: [45] Copyright (2022) the American Chemical Society. (d) N₂-plasma-treatment synthesis, (e) SEM, and (f) CV in 1.0 M KOH of N-Pd₆₀Cu₄₀ NS. "Reproduced with permission from Ref.: [46] Copyright (2022) Wiley-VCH". (g) SEM and (h) CV in 1.0 M KOH of PdNi. "Adapted with permission from Ref.: [47] Copyright (2023) Elsevier".

foam-like PdM nanostructures with interconnected nanosheets proved by SEM (Figure 3g), PdNi with more accessible active sites, improved electron mobility and low synergism gave a great CO_{Oxid} activity in 1.0 M KOH at $E_{\text{Oxid}}/j_{\text{Oxid}}$ ($-0.200_{\text{Ag/AgCl}}/1.88 \text{ mA/cm}^2$, Figure 3h) compared to PdFe ($-0.18_{\text{Ag/AgCl}}/1.45 \text{ mA/cm}^2$) and PdCo ($-0.17_{\text{Ag/AgCl}}/1.04 \text{ mA/cm}^2$). Dispersion of Ir-single-atom-doped on Pd nanoparticles (Ir-SAs/Pd) via chemical reduction with ascorbic acid (AA), which showed superior CO_{Oxid} in 1.0 M KOH at lower $E_{\text{onset}}/E_{\text{Oxid}}$ ($-0.601/-0.20 \text{ V}_{\text{SCE}}$) than Pd ($-0.376/-0.18 \text{ V}_{\text{SCE}}$), owing to the improved electron density and down-shifted d-band center of Pd by Ir doping, proven by DFT simulations.^[48] The low CO_{Oxid} activity of the self-standing PdM nanostructures may be traced to their low conductivity without any conductive materials like carbon.

Ternary Pd-based electrocatalysts, including PdM with metal-oxide/carbon-based supports, have recently shown

excellent CO_{Oxid} activity traced to the contributory/synergistic effects with the metal-oxide/carbon supports. Sol-gel/impregnation (80°C ; 24 h) methods (Figure 4a) were employed to prepare PdNiO nanocrystals anchored CeO₂/ion-like carbon (PdNiO-CeO₂/OLC), where the CeO₂/OLC acted as nanoreactor for the growth of PdNiO with spongy-like Pd on flower-like CeO₂/OLC that exhibited strong electronic interaction, evidenced by HRTEM (Figure 4b) that eased CO adsorption/activation and generated activated OH^- species needed for its high CO_{Oxid} by at least 1.66-folds of PdNiO/OLC, 1.88-folds of PdNiO-CeO₂ and 2.12-folds of commercial-Pd/C in 0.1 M HClO₄, 0.1 M KOH, and 0.1 M NaHCO₃ media (Figures 4c-3e).^[49] However, the use of CeO₂/carbon black (CB) in PdNiO-CeO₂/CB with Pd nanospheres on flake-like CeO₂/CB required lower energy for slightly enhanced CO_{Oxid} kinetics than PdNiO-CeO₂/OLC in the three electrolytes.^[50] Combining metal oxide with

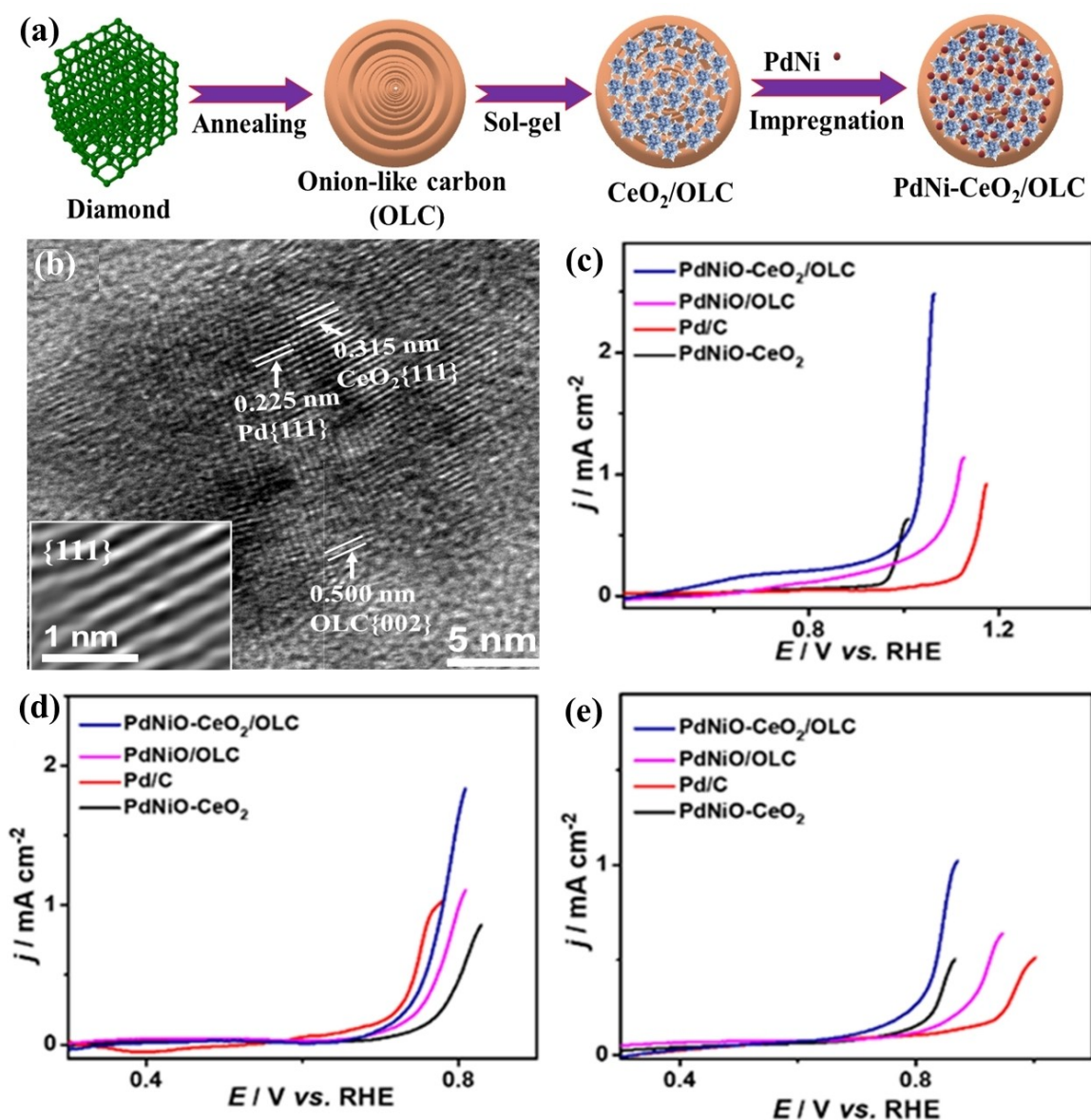


Figure 4. (a) Sol-gel/impregnation synthetic scheme, (b) HRTEM, CV curves in (c) 0.1 M HClO₄, (d) 0.1 M KOH and (e) 0.1 M NaHCO₃ of PdNiO-CeO₂/OLC. "Reproduced with permission from Ref.: [49] Copyright (2023) the Royal Society of Chemistry".

O₂-rich and carbon is preferred for Pd-based catalysts in improving the CO_{oxid} electrocatalysis.

4. Conclusions and Future Perspectives

This work presents the recent synthesis strategies for Pd-based catalysts with distinct morphologies for electrochemical CO_{oxid} in different electrolytes. The chemical-reduction method is the most promising for controlling the fabrication of self-standing/supported Pd-based catalysts under ambient conditions. Au/Pd/gC₃N₄NTs exhibited outstanding CO_{oxid} in 0.1 M KOH in terms of j_{Oxid} (15.5 mA/cm²), followed by PtPd/CNs (14.75 mA/cm²), due to the combined physicochemical merits of gC₃N₄ and catalytic features of metals. Remarkably, there are few studies on Pd-based catalysts for electrochemical CO_{oxid}, which cannot optimize the catalytic performance of Pd-based catalysts and there are various problems that need to be solved, including the performance-indicator parameters remaining ambiguous. The high cost, rarity, and high Pd-loading (up to 30 wt.%) remain a grand challenge. Also, the inferior yield of the current preparation methods and their related multiple reaction steps cannot meet the practical applications. Meanwhile, the effect of electrolyte type, pH, and concentration on the electrocatalytic performance of Pd-based catalysts is not studied yet.

The future perspectives to solve the current drawbacks in Pd-based catalysts include utilizing Pd-atomically doped supports at low loading (0.5–2.5 wt.%), which could decrease the cost significantly and enhance the CO_{oxid} catalytic activity, due to the quantum size effect and maximized atom utilization. The in-situ fabrication of Pd-based catalysts with carbon materials as supports (i.e., C₃N₄, MOF, nickel foam, carbon cloth, and activated carbon) can enhance the yield of Pd and allow in-situ anchorage on conductive substrates. Also, combined experimental and theoretical studies are needed to corroborate the effects of electrolytes, besides Pd shapes and compositions on the electrochemical CO_{oxid}.

Acknowledgements

KI Ozoemena thanks the *ChemElectroChem* team for the invitation to write this mini-review as part of their Special Collection on *Electrochemistry in Africa*. This work was supported by the DSI/NRF/Wits SARChI Chair in Materials Electrochemistry and Energy Technologies (MEET) (UID No.132739), Qatar University High Impact Internal Grant (QUHI-CAM-22/23-550), and Qatar National Research Fund (QUHI-CAM-22/23-550). Open Access funding was provided by the Qatar National Library.

Conflict of Interests

The authors declare no conflict of interest.

Data Availability Statement

The data that support the findings of this study are available from the corresponding author upon reasonable request.

Keywords: Electrocatalysis · Carbon monoxide oxidation · Palladium-based catalysts

- [1] R. M. Al Soubaihi, K. M. Saoud, M. T. Z. Myint, M. A. Göthelid, J. Dutta, *Catalysts* **2021**, *11*, 131.
- [2] K. Eid, A. Gamal, A. M. Abdullah, *Green Chem.* **2023**, *25*, 1276–1310.
- [3] A. K. Ipadeola, M. Chitt, A. Abdelgawad, K. Eid, A. M. Abdullah, *Int. J. Hydrogen Energy* **2023**, *48*, 17434–17467.
- [4] J. Wu, D. Chen, J. Chen, H. Wang, *J. Phys. Chem. C* **2023**, *127*, 6262–6270.
- [5] K. Eid, M. H. Sliem, M. Al-Ejji, A. M. Abdullah, M. Harfouche, R. S. Varma, *ACS Appl. Mater. Interfaces* **2022**, *14*, 40749–40760.
- [6] A. Abdelgawad, B. Salah, K. Eid, A. M. Abdullah, R. S. Al-Hajri, M. Al-Abri, M. K. Hassan, L. A. Al-Sulaiti, D. Ahmadaliev, K. I. Ozoemena, *Int. J. Mol. Sci.* **2022**, *23*, 15034.
- [7] A. K. Ipadeola, B. Salah, A. Ghanem, D. Ahmadaliev, M. A. Sharaf, A. M. Abdullah, K. Eid, *Heliyon* **2023**, *9*, e16890.
- [8] A. K. Ipadeola, K. Eid, A. K. Lebechi, A. M. Abdullah, K. I. Ozoemena, *Electrochem. Commun.* **2022**, *140*, 107330.
- [9] K. I. Ozoemena, *RSC Adv.* **2016**, *6*, 89523–89550.
- [10] Y. Zuo, D. Rao, S. Li, T. Li, G. Zhu, S. Chen, L. Song, Y. Chai, H. Han, *Adv. Mater.* **2018**, *30*, 1704171.
- [11] B. Salah, A. K. Ipadeola, A. M. Abdullah, K. Eid, *ACS Appl. Eng. Mater.* **2023**, *1*, 2196–2206. 10.1021/acsaenm.3c00281.
- [12] B. Salah, A. K. Ipadeola, A. M. Abdullah, A. Ghanem, K. Eid, *Int. J. Mol. Sci.* **2023**, *24*, 11832.
- [13] J. J. Ogada, A. K. Ipadeola, P. V. Mwonga, A. B. Haruna, F. Nichols, S. Chen, H. A. Miller, M. V. Pagliaro, F. Vizza, J. R. Varcoe, D. M. Meira, D. M. Wamwangi, K. I. Ozoemena, *ACS Catal.* **2022**, *12*, 7014–7029.
- [14] N. E. Mphahlele, A. K. Ipadeola, A. B. Haruna, P. V. Mwonga, R. M. Modibedi, N. Palaniyandy, C. Billing, K. I. Ozoemena, *Electrochim. Acta* **2022**, *409*, 139977.
- [15] A. K. Ipadeola, P. V. Mwonga, S. C. Ray, R. R. Maphanga, K. I. Ozoemena, *ChemElectroChem* **2020**, *7*, 4562–4571.
- [16] A. K. Ipadeola, N. Z. Lisa Mathebula, M. V. Pagliaro, H. A. Miller, F. Vizza, V. Davies, Q. Jia, F. Marken, K. I. Ozoemena, *ACS Appl. Eng. Mater.* **2020**, *3*, 8786–8802.
- [17] A. K. Ipadeola, K. I. Ozoemena, *RSC Adv.* **2020**, *10*, 17359–17368.
- [18] B. N. Grgur, N. M. Marković, C. A. Lucas, P. N. Ross Jr, *J. Serb. Chem. Soc.* **2001**, *66*, 785–797.
- [19] Y. Zhou, Z. Wang, C. Liu, *Catal. Sci. Technol.* **2015**, *5*, 69–81.
- [20] A. M. Gomez-Marin, J. P. Hernandez-Ortiz, *J. Phys. Chem. C* **2014**, *118*, 2475–2486.
- [21] H. Tan, Y.-P. Xu, S. Rong, R. Zhao, H. Cui, Z.-N. Chen, Z.-N. Xu, N.-N. Zhang, G.-C. Guo, *Nanoscale* **2021**, *13*, 18773–18779.
- [22] J. Spendelov, J. Goodpaster, P. Kenis, A. Wieckowski, *J. Phys. Chem. B* **2006**, *110*, 9545–9555.
- [23] C. Stoffelsma, P. Rodriguez, G. Garcia, N. Garcia-Araez, D. Strmcnik, N. M. Marković, M. T. Koper, *J. Am. Chem. Soc.* **2010**, *132*, 16127–16133.
- [24] J. Fan, H. Du, Y. Zhao, Q. Wang, Y. Liu, D. Li, J. Feng, *ACS Catal.* **2020**, *10*, 13560–13583.
- [25] C. Zhu, D. Du, A. Eychmüller, Y. Lin, *Chem. Rev.* **2015**, *115*, 8896–8943.
- [26] A. Gamal, K. Eid, A. M. Abdullah, *Int. J. Hydrogen Energy* **2022**, *47*, 5901–5928.
- [27] Q. Lu, X. Zhao, R. Luque, K. Eid, *Coord. Chem. Rev.* **2023**, *493*, 215280.
- [28] D. Wang, P. Wang, S. Wang, Y.-H. Chen, H. Zhang, A. Lei, *Nat. Commun.* **2019**, *10*, 2796.
- [29] X. Zhao, P. Pachfule, A. Thomas, *Chem. Soc. Rev.* **2021**, *50*, 6871–6913.
- [30] S. i. Yamazaki, M. Asahi, Z. Siroma, T. Ioroi, *ChemCatChem* **2020**, *12*, 2717–2720.
- [31] J. M. Solomon, S. Pachamuthu, J. J. Arulanandan, N. Thangavel, R. Sathyamurthy, *Environ. Sci. Pollut. Res. Int.* **2020**, *27*, 32229–32238.
- [32] H. Kim, T. Y. Yoo, M. S. Bootharaju, J. H. Kim, D. Y. Chung, T. Hyeon, *Adv. Sci.* **2022**, *9*, 2104054.
- [33] S. H. Gebre, M. G. Sendeku, *J. Energy Chem.* **2022**, *65*, 329–351.
- [34] H. Wang, S. Yin, Y. Li, H. Yu, C. Li, K. Deng, Y. Xu, X. Li, H. Xue, L. Wang, *J. Mater. Chem. A* **2018**, *6*, 3642–3648.

- [35] Y. Yang, Y. Cao, L. Yang, Z. Huang, N. V. Long, *Nanomaterials* **2018**, *8*, 208.
- [36] F. Gao, Y. Zhang, Z. Wu, H. You, Y. Du, *Coord. Chem. Rev.* **2021**, *436*, 213825.
- [37] A. K. Ipadeola, K. Eid, A. M. Abdullah, K. I. Ozoemena, *Langmuir* **2022**, *38*, 11109–11120.
- [38] A. K. Ipadeola, K. Eid, A. M. Abdullah, R. S. Al-Hajri, K. I. Ozoemena, *Nanoscale Adv.* **2022**, *4*, 5044–5055.
- [39] B. Salah, K. Eid, A. M. Abdelgwad, Y. Ibrahim, A. M. Abdullah, M. K. Hassan, K. I. Ozoemena, *Electroanalysis* **2022**, *34*, 677–683.
- [40] K. Eid, M. H. Sliem, A. M. Abdullah, *Nanoscale* **2019**, *11*, 11755–11764.
- [41] K. Eid, M. H. Sliem, H. Al-Kandari, M. A. Sharaf, A. M. Abdullah, *Langmuir* **2019**, *35*, 3421–3431.
- [42] X. Qi, X. Gong, N. Ye, Z. Jiang, T. Fang, *Int. J. Hydrogen Energy* **2022**, *47*, 27527–27540.
- [43] T. Zeng, L. Zheng, H. Chen, Y. Wang, M. Ling, S. Sun, F. Zhang, W. Yuan, L. Y. Zhang, *Colloids Surf. A Physicochem. Eng. Asp.* **2023**, *656*, 130358.
- [44] E. Plaza-Mayoral, I. J. Pereira, K. Nicole Dalby, K. D. Jensen, I. Chorkendorff, H. Falsig, P. Sebastián-Pascual, M. Escudero-Escribano, *ACS Appl. Energ. Mater.* **2022**, *5*, 10632–10644.
- [45] C. Shen, H. Chen, M. Qiu, Y. Shi, W. Yan, Q. Jiang, Y. Jiang, Z. Xie, *J. Mater. Chem. A* **2022**, *10*, 1735–1741.
- [46] X. Meng, T. Zeng, S. Ma, L. Zheng, H. Chen, W. Yuan, L. Y. Zhang, *Adv. Mater. Interfaces* **2022**, *9*, 2101849.
- [47] A. K. Ipadeola, A. Abdelgwad, B. Salah, A. Ghanem, M. Chitt, A. M. Abdullah, K. Eid, *Int. J. Hydrog. Energy* **2023**, 10.1016/j.ijhydene.2023.04.149.
- [48] X. Wei, J. Zhang, C. Liu, X. Han, Y. Deng, W. Hu, *Part. Part. Syst. Charact.* **2022**, *39*, 2200013.
- [49] A. K. Ipadeola, A. B. Haruna, A. M. Abdullah, R. S. Al-Hajri, R. Viter, K. I. Ozoemena, K. Eid, *Catal. Sci. Technol.* **2023**, *13*, 3035–3046.
- [50] A. K. Ipadeola, A. B. Haruna, A. M. Abdullah, M. F. Shibl, D. Ahmadaliev, K. I. Ozoemena, K. Eid, *Catal. Today* **2023**, *421*, 114178.

Manuscript received: July 27, 2023

Revised manuscript received: September 3, 2023

Version of record online: November 15, 2023